

Corner wetting in a far-from-equilibrium magnetic growth model

Virginia Manías¹, Julián Candia^{1,2} and Ezequiel V. Albano³

¹ IFLP, CONICET/Departamento de Física, Universidad Nacional de La Plata, C.C. 67, 1900 La Plata, Argentina

² The Abdus Salam International Centre for Theoretical Physics, Strada Costiera 11, 34014 Trieste, Italy

³ INIFTA, Universidad Nacional de La Plata, CONICET, C.C. 16, Sucursal 4, 1900 La Plata, Argentina

Received:

Abstract. The irreversible growth of magnetic films is studied in three-dimensional confined geometries of size $L \times L \times M$, where $M \gg L$ is the growing direction. Competing surface magnetic fields, applied to opposite corners of the growing system, lead to the observation of a localization-delocalization (weakly rounded) transition of the interface between domains of up and down spins on the planes transverse to the growing direction. This effective transition is the precursor of a true far-from-equilibrium corner wetting transition that takes place in the thermodynamic limit. The phenomenon is characterized quantitatively by drawing a magnetic field-temperature phase diagram, firstly for a confined sample of finite size, and then by extrapolating results, obtained with samples of different size, to the thermodynamic limit. The results of this work are a nonequilibrium realization of analogous phenomena recently investigated in equilibrium systems, such as corner wetting transitions in the Ising model.

PACS. 68.08.Bc Wetting – 68.35.Rh Phase transitions and critical phenomena – 05.70.Ln Nonequilibrium and irreversible thermodynamics – 75.70.Cn Magnetic properties of interfaces

1 Introduction

Certainly, the phenomenon of wetting is a problem of primary importance in many fields of practical technological applications (such as lubrication, efficiency of detergents, oil recovery in porous materials, stability of paint coatings, interaction of macromolecules with interfaces, etc.

[1]), while it is also an attractive, challenging phenomenon from the theoretical point of view. Indeed, many theoretical efforts involving different approaches have been devoted to the study of wetting transitions at interfaces under equilibrium conditions [2,3,4,5,6,7,8,9,10,11] (for general overviews of the subject see e.g. [12,13]), and more

recently some investigations on nonequilibrium wetting phenomena [14,15,16] have been carried out as well.

A related phenomenon, which has attracted great interest in the past decade, is the so-called filling or corner wetting transition of a fluid adsorbed on a wedge [17,18,19]. At present, it is experimentally feasible to control the shape of solid surfaces at a nanoscopic level, and indeed a growing variety of new types of interfacial phase transitions have been found in fluids confined by such structured substrates [20]. The critical wetting in 2D [21,22,23,24,25,26] and 3D [27,28] wedges has also recently been investigated theoretically under equilibrium conditions. In particular, it should be mentioned that the exact solution for a two-dimensional rectangular Ising ferromagnet forming a corner with a surface field applied to the spins on edges has recently been obtained [26]. Furthermore, many theoretical results have later been corroborated by extensive Monte Carlo simulations performed in both 2D [29] and 3D [30].

Within the context of these recent developments, the aim of this work is to investigate the phenomenon of corner wetting under far-from-equilibrium conditions by means of a Monte Carlo approach. To our best knowledge, this paper presents the first study of nonequilibrium wedge wetting. It is also worth mentioning that the irreversible filling of cavities with magnetic materials is also a frontier topic in the field of the physics of new materials, since modern trends in technology [31] require the characterization of the filling of templates, containing imprinted nanometer/micrometer sized features, with a depositing material [32,33].

2 Brief summary of recent studies on corner wetting under equilibrium.

Since the present work addresses the phenomena of non-equilibrium corner wetting in a magnetic material, it is useful to briefly describe recent progress in the study of their equilibrium counterpart [21,22,23,24,25,26,27,28,29,30]. Figure 1 shows a sketch of the corner geometry, of size $L \times L$, used for the study of corner wetting in two dimensions. Of course, the same sketch can be considered as a transverse view of a three dimensional array of size $L \times L \times M$ (with $M \gg L$), as used in the present work.

Let us consider a wedge in contact with the gas phase of a fluid at temperature T and chemical potential μ . Based on thermodynamic (macroscopic) arguments [22], the theory of corner wetting predicts that the filling of the wedge by the fluid occurs at the transition temperature T_f , given by [22,23]

$$\Theta_\pi(T_f) = \pi/2 - \phi, \quad (1)$$

where Θ_π [34] is the contact angle describing the droplets on a planar interface in the regime of incomplete wetting and ϕ is the angle between the wall and the diagonal of the wedge (see Figure 1). Consequently, T_f is smaller than the wetting temperature T_w characterising the liquid-vapour interaction on a planar substratum.

Similar arguments can be drawn for a magnetic system in a wedge geometry, such as the Ising magnet in the square lattice in the presence of competing confinement fields as shown in Figure 1. For the sake of simplicity,

let us discuss the filling transition (also known as corner-wetting transition) in $d = 2$ considering the case $\phi = \pi/4$ only. The transition is of second-order and occurs at a critical field H_{cw} [26], which depends on T , and it is observed at temperatures below the order-disorder Onsager critical temperature of the Ising magnet. At low temperatures, the interface remains bounded to one wall and its mean distance to the corner ($\langle l_o \rangle$, see Figure 1) diverges according to a power-law behavior when approaching the transition. Of course, the growth of the correlation lengths is bound by the finite lattice size and true divergences are only possible in the thermodynamic limit. So, one has

$$\langle l_o \rangle \propto t^{-\beta_s}, \quad t = H_{cw}(T) - H, \quad (2)$$

where $\beta_s = 1$ is the order parameter critical exponent. The interface also develops correlations along the directions parallel and perpendicular to it (see Figure 1). The corresponding correlation lengths (ξ_x and ξ_\perp , respectively), also diverge at the critical point according to

$$\xi_x \propto t^{-\nu_x}, \quad \xi_\perp \propto t^{-\nu_\perp}, \quad (3)$$

where the correlation length exponents are $\nu_x = 1$ and $\nu_\perp = 1$, respectively.

On the other hand, taking first the limit $L \rightarrow \infty$ and then the limit $t \rightarrow 0^+$, the probability distribution of the mean position of the interface is expected to decay exponentially, namely

$$P(\langle l_o \rangle) = \frac{1}{\langle l_o \rangle} \exp\left(-\frac{l_o}{\langle l_o \rangle}\right), \quad t \rightarrow 0^+. \quad (4)$$

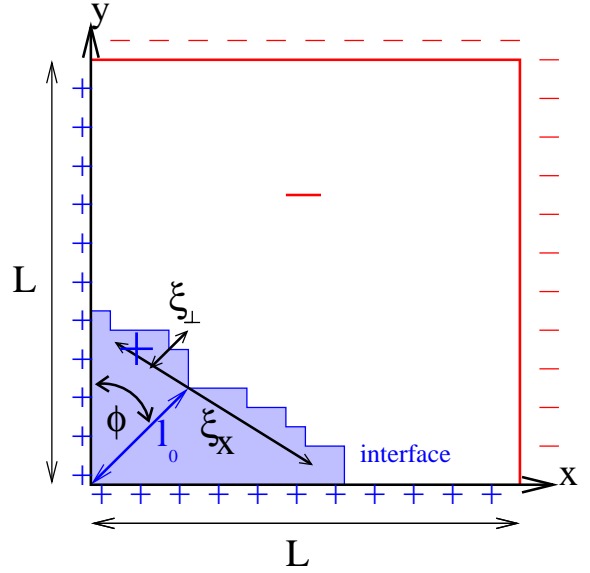


Fig. 1. Sketch of the simulation geometry where a transverse plane ($k = \text{constant}$) of size $L \times L$ of the square lattice is shown. Free boundary conditions are used for the spins in rows $i = 1, i = L$ and $j = 1, j = L$, with integers $(i, j) \in [1, L]$ labelling the lattice sites. Additionally, a magnetic field H acts on all spins in the rows $i = 1$ and $j = 1$, while a magnetic field $-H$ acts on all spins in the rows $i = L$ and $j = L$. A typical configuration of the system below the critical point then contains an interface between a domain of positive magnetization (+) and a domain with negative magnetization (-). Fluctuations of the interface are characterised by correlation lengths ξ_x and ξ_\perp in the directions parallel and perpendicular to the interface, respectively.

For finite systems of side L , equation (4) needs to be symmetrized with respect to both corners to which the interface can be bound [29]. Equation (4) holds within the regime of incomplete corner wetting (or equivalently to the case of incomplete corner filling, when the interface of the magnetic domain filling the sample is still bound to one corner far from the diagonal crossing the sample from

left-top to right-bottom (1)). However, in the regime of complete corner wetting (or equivalently complete filling), $t < 0$, the average location of the interface lies along the diagonal taken from the upper-left corner to the lower right corner. So, one has $\langle l_o \rangle = L/\sqrt{2}$ and the probability distribution becomes

$$P(\langle l_o \rangle) \propto \exp\left(-\frac{[l_o - \langle l_o \rangle]^2}{2\xi_{\perp}^2}\right), \quad (5)$$

with [23]

$$\xi_{\perp} \propto L^{\frac{1}{2}}, \quad (6)$$

since it can be interpreted in terms of a random walk description of the interface in $d = 2$, such that excursions in the direction perpendicular to the average interface orientation add up randomly [35].

Equation (5) implies that for complete wetting, the average magnetization vanishes ($\langle m \rangle = 0$) and the Gaussian distribution of the interface location translates into a Gaussian distribution of the magnetization given by

$$P(m) \sim \exp\left(-\frac{m^2 L^2}{2k_B T \chi_L}\right), \quad (7)$$

with

$$\chi_L \propto \xi_{\perp}^2 \propto L, \quad (8)$$

where the size-dependent width of the Gaussian is given by $\chi_L \equiv (\langle m^2 \rangle - \langle m \rangle^2)$, with $\langle m \rangle^2 = 0$ within the complete wetting regime. It should be noticed that, as in the case of the localization-delocalization transition observed for the Ising magnet in a slit geometry [2,44], in the case of

complete wetting the interface is no longer bound to the wall (or corner, respectively).

3 The Magnetic Eden Model in a corner geometry and the simulation method

For definiteness, we will adopt a magnetic language throughout, although the relevant physical concepts discussed here can be extended to other systems such as fluids, polymers, and binary mixtures. The irreversible growth of a ferromagnetic material has been studied by using the so-called magnetic Eden model (MEM) [36], an extension of the classical Eden model [37] in which the growing particles have an additional degree of freedom, i.e., the spin. Several recent investigations based on this model showed a rich variety of interesting phenomena, such as the occurrence of morphological phase transitions associated with the growing interface [38], Ising-like order-disorder phase transitions [39], spontaneous magnetization reversals [40], and a far-from-equilibrium wetting transition driven by competing surface magnetic fields [15,16].

The MEM in $(2 + 1)$ -dimensions is studied in the square lattice by using a rectangular geometry $L \times L \times M$ (with $M \gg L$). The location of each spin on the lattice is specified through its coordinates (i, j, k) , ($1 \leq i, j \leq L$, $1 \leq k \leq M$). A transverse plane of the used geometry, taken for $k = \text{constant}$, is sketched in Figure 1. The starting seed for the growing cluster is a plane of $L \times L$ parallel-oriented spins placed at $k = 1$, and cluster growth takes place along the positive longitudinal direction (i.e., $k \geq 2$).

Open boundary conditions are adopted in both transverse directions, and competing surface magnetic fields $H > 0$ and $H' = -H$ are applied to opposite corners, as shown in Figure 1. Then, clusters are grown by selectively adding spins ($S_{ijk} = \pm 1$) to perimeter sites, which are defined as the nearest-neighbour (NN) empty sites of the already occupied ones. Considering a ferromagnetic interaction of strength $J > 0$ between NN spins, the energy E of a given configuration of spins is given by

$$E = -\frac{J}{2} \left(\sum_{\langle ijk, i'j'k' \rangle} S_{ijk} S_{i'j'k'} \right) - H \left(\sum_{\langle jk \rangle} S_{1jk} + \sum_{\langle ik \rangle} S_{i1k} \right) + H \left(\sum_{\langle jk \rangle} S_{Ljk} + \sum_{\langle ik \rangle} S_{iLk} \right) \quad (9)$$

where the summation $\langle ijk, i'j'k' \rangle$ is taken over occupied NN sites, while the remaining terms are sums over occupied surface sites, in order to take into account the effect of the surface magnetic fields. The Boltzmann constant is set equal to unity throughout, and the temperature, energy, and magnetic fields are measured in units of J . The probability for a perimeter site to be occupied by a spin is taken as proportional to the Boltzmann factor $\exp(-\frac{\Delta E}{T})$, where ΔE is the change of energy involved in the addition of the spin. At each step, the probabilities of adding up and down spins to a given site have to be evaluated for all perimeter sites. After proper normalization of the probabilities, the growing site and the orientation of the spin are determined with Monte Carlo techniques. For additional details on the MEM and the simulation method see e.g. [15,16,36,38,40].

Since the observables of interest (e.g. the mean transverse magnetization and its fluctuations, see below) require the growth of samples with a large number of transverse planes of size $L \times L$, clusters having up to 10^9 spins have typically been grown for lattice sizes in the range $12 \leq L \leq 96$. It should be mentioned that the growing front leaves voids behind that are incorporated to the bulk of the sample during some transient period. However, since these voids are also perimeter sites they are ultimately filled in during the growth process. Hence, far behind the active growth interface, the system is compact and frozen. So, the different quantities of interest are measured on defect-free transverse planes.

Moreover, the update algorithm is quite time consuming, as compared to standard Ising simulations, since the growing probability has to be computed after each deposition event. Hence, it should be noticed that the results obtained in this work involve a large computational effort. Let us also remark that, although both the interaction energy and the Boltzmann probability distribution considered for the MEM are similar to those used for the Ising model with surface magnetic fields, these two models operate under extremely different conditions, since the MEM describes the irreversible growth of a magnetic material, while the Ising model deals with a magnet under equilibrium. Previous studies have demonstrated that the MEM in $(1+1)$ -dimensions is not critical but exhibits a second-order transition at $T_c = 0.69 \pm 0.01$ in $(2+1)$ -dimensions [39].

4 Results and discussion

The growth of magnetic Eden aggregates in a $(d+1)$ -confined geometry is characterized by an initial transient period followed by a nonequilibrium stationary state that is independent of the initial configuration [15]. The length of the transient is of the order of L^d ($d = 2$ in the present study), and the proportionality constant depends on T . We have checked that disregarding the first $100L^2$ transverse planes, subsequent averages are independent of the initial configuration. So, all results reported in this paper are obtained under these conditions.

Depending on the temperature and the surface magnetic field considered, different regimes are clearly distinguished upon growth of a magnetic aggregate in the confined corner geometry, as illustrated by the typical snapshot configurations of transverse ($k = \text{constant}$) planes shown in Figure 2. Furthermore, in order to characterize these different phases quantitatively, we will locate the boundaries between them in a magnetic field *versus* temperature ($H - T$) phase diagram (see Figure 3). Below, we will first describe the results for a confined, finite-size system, and then we will obtain the phase diagram in the thermodynamic limit by means of extrapolation procedures.

Let us now discuss the localization-delocalization behavior of the interface observed when the value of the surface field is fixed ($H = 0.4$) but the temperature is increased. For this qualitative description we will use the typical snapshot configurations shown in Figure 2. Figure 2(a) shows the regime characteristic of low temperatures

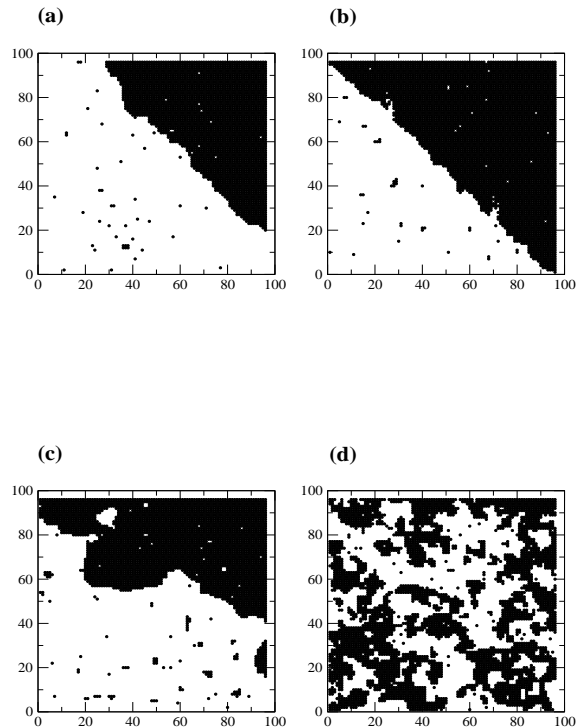


Fig. 2. Typical snapshot configurations of transverse ($k = \text{constant}$) planes. Black points correspond to down spins, while up spins are left in white. The surface field is positive (negative) on the left and bottom (right and top) sides of the wedge, as shown in Figure 1. The snapshots correspond to lattices of size $L = 96$ and are obtained keeping the surface fields constant and varying the temperature, as follows: (a) $H = 0.4$, $T = 0.6$; (b) $H = 0.4$, $T = 0.65$, (c) $H = 0.4$, $T = 0.7$, and (d) $H = 0.4$, $T = 1.0$.

(i.e. far below the critical temperature of the MEM). Here, the interface between up and down domains is localized close to the upper-right corner. Of course, during very long-time simulations one observes the localization of the interface close to both corners with the same probability. Keeping the same field but increasing the temperature, the interface starts to depart from the corners and, close

to the effective corner wetting transition temperature of the considered lattice, it remains still localized close to the diagonal of the sample, as shown in Figure 2(b). However, further increase of the temperature causes the interface to become delocalized (see Figure 2(c)). Here the domain of positive spins makes frequent excursions up to the boundary with negative field (see the lower-right corner of Figure 2(c)). Also, notice that a relatively weaker excursion of the negative domain to the positive boundary field is observed at the upper-left corner. Of course, due to the symmetry of the system, these excursions cause the temporal average position of the interface to be just at the diagonal of the sample with $\langle l_o \rangle = L/\sqrt{2}$, while its probability distribution is given by equation (5). For this regime the total magnetization vanishes and its probability distribution is a Gaussian centered around $m = 0$, see equation (7). Finally, at higher temperatures and within the disordered phase (i.e., above the critical temperature of the MEM), the interface between domains of up and down spins vanishes due to the thermal noise, as shown by the typical high-temperature configuration of Figure 2(d).

Let us now discuss the interface localization-delocalization “phase diagram” of a confined system of lateral size $L = 12$, as shown in Figure 3.

In order to locate the transition curve we have measured the magnetization fluctuations, given by

$$\chi(L, T) = \frac{L^2}{T} (\langle m^2 \rangle - \langle |m| \rangle^2) , \quad (10)$$

where $\langle \dots \rangle$ means the average taken over a large number of transverse planes in the stationary regime, and $m = m(k, L, T, H)$ is the mean transverse magnetization given

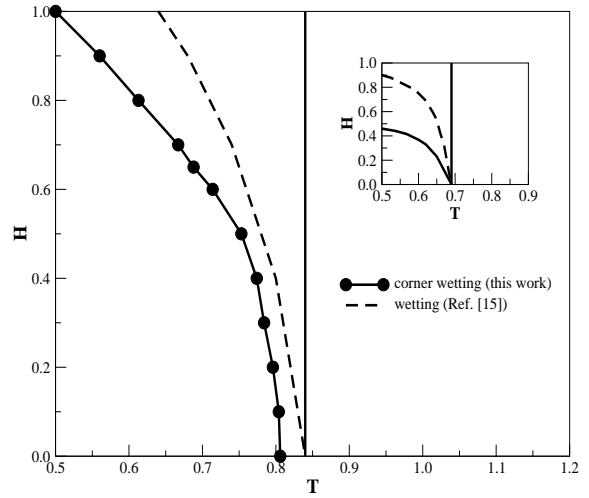


Fig. 3. The $H - T$ phase diagram corresponding to a lattice of size $L = 12$. The vertical straight line at $T_c(L) = 0.84$ shows the L -dependent critical temperature of the MEM in the absence of any magnetic field, which separates the low-temperature ordered phase from the high-temperature disordered phase. Besides, the corner localization-delocalization transition curve (full circles and solid line) obtained in this work, as well as the localization-delocalization transition curve (dashed line) that corresponds to the MEM with competing surface magnetic fields applied to parallel confinement walls [15], is shown for comparison. The inset shows the phase diagram corresponding to the thermodynamic limit, as obtained by extrapolating results obtained for systems of different lattice size. Again, the corner wetting transition (solid line) is compared to the wetting transition of the MEM (dashed line) obtained in Reference [15]. More details in the text.

by

$$m = \frac{1}{L^2} \sum_{i,j=1}^L S_{ijk} . \quad (11)$$

It should be noticed that under equilibrium conditions and provided that the fluctuation-dissipation theorem holds, the fluctuations of the magnetization can be

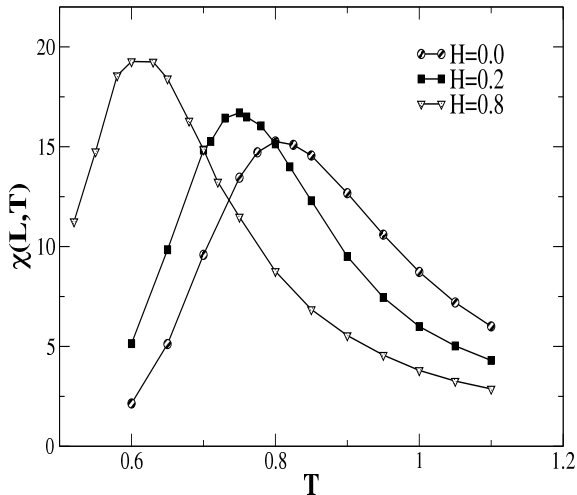


Fig. 4. Plots of the magnetization fluctuations as a function of the temperature obtained for different values of the magnetic field, as indicated. Following a standard procedure [44], the maxima of $\chi(L, T)$ define the points of the corner localization-delocalization transition curve on the $H - T$ plane, as shown in Figure 3.

identified with the susceptibility. However, this may not be the case for the present far-from-equilibrium system.

Working under equilibrium [41] and far from it [40,42,43] is usual to locate L -dependent ‘critical’ points at the maximum of $\chi(L, T)$. This procedure has proved to be also useful to locate L -dependent localization-delocalization transition points (namely wetting “critical” temperatures $T_{cw}(L)$) under equilibrium [44] and far from it [15]. So, we have also used the same method in the present case. In order to illustrate this procedure, Figure 4 shows plots of $\chi(L, T)$ as a function of the temperature for different values of the surface magnetic field. The maximum of each curve defines a point in the transition curve shown in Figure 3. It should be noticed that the localization-delocalization transition in a confined system actually cor-

-from-equilibrium magnetic growth model

responds to a so-called quasi-corner wetting transition, which is indeed the precursor of the true corner wetting transition that occurs in the thermodynamic limit.

In Figure 3, the vertical straight line at $T_c(L = 12) = 0.84$ shows the location of the L -dependent “critical” temperature of the finite system in the absence of surface fields. This value was obtained previously for the MEM in the absence of an external magnetic field and corresponds to the slit geometry [39]. Although, as it is well known from finite-size scaling theory, there is some degree of arbitrariness in locating the L -dependent critical temperature $T_c(L)$ of a finite system, the actual critical point T_c of the infinite system, which can be obtained by extrapolating $T_c(L)$ to the $L \rightarrow \infty$ limit, is unique and independent of any particular choice for the finite-size critical point. Let us also recall that for low temperatures ($T < T_c(L)$) the phase diagram corresponds to the ordered growth regime, while high temperatures ($T \geq T_c(L)$) are associated with the disordered growth regime.

For the sake of comparison, the localization-delocalization transition curve obtained in this work for the corner geometry is compared to the localization-delocalization transition curve of the MEM (dashed line in Figure 3) that corresponds to competing surface magnetic fields applied to parallel confinement walls [15], i.e., the so-called slit geometry. Notice that in this case the critical curve ends, for $H = 0$, at the L -dependent critical point $T_c(L = 12) = 0.84$. It is observed that the phase diagrams obtained here are similar to the analogous phenomena of wetting and corner wetting observed in 2D equilibrium systems, as e.g.

in the confined Ising model [29,44]. In fact, for a given surface field, in the case of corner wetting, the corresponding critical temperature is always smaller than for pure wetting except, of course, for $H = 0$. This scenario is in agreement with equation (1), which was obtained on the basis of thermodynamic (equilibrium) considerations [22].

It should be noticed that the transition curve corresponding to the corner geometry intercepts the horizontal axis ($H = 0$) close to $T_c(L = 12) \simeq 0.81$, i.e., a value slightly smaller than the L -dependent order-disorder critical temperature of the MEM model in the absence of surface fields. This shift simply reflects the different boundary conditions that one has to use to study both systems. In fact, for the corner geometry one has to apply open boundary conditions, while for studying the confinement due to parallel walls one has to adopt open (periodic) boundary conditions along (in the direction perpendicular to) the walls. Of course, both localization-delocalization transitions lie within the ordered growth regime where an interface between domains is well defined.

Further insights can be gained by examining the behavior of the probability distribution of the mean transverse magnetization, $P_L(m)$. In fact, in the thermodynamic limit, the order parameter probability distribution of an equilibrium system at criticality is universal (up to rescaling of the order parameter), and hence it contains information on the universality class of the system [45,46,47]. Figure 5 shows the dependence of $P_L(m)$ on the surface magnetic field for fixed values of the temperature ($T = 0.65$) and the lattice size ($L = 12$). For larger

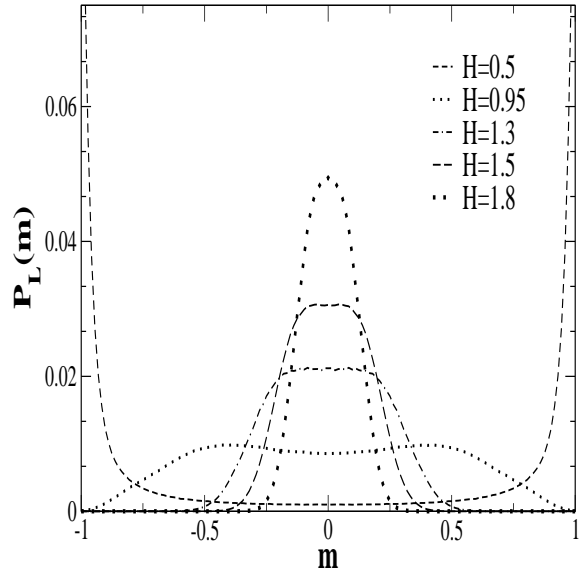


Fig. 5. Order parameter probability distributions obtained for $T = 0.65$ and different values of the field, as indicated. The lattice size is $L = 12$.

fields ($H = 1.8$ in Figure 5) the distribution is a Gaussian centered at $m = 0$, in agreement with the fact that the **average** location of the interface (for temperatures below $T_c(L)$) is a straight line crossing the sample from one corner, where the magnetic fields have opposite direction, to the other (see e.g. the snapshots shown in Figures 2 (b) and (c), as well as the corresponding discussion). Hence, the average magnetization $\langle m \rangle = 0$, and the Gaussian distribution of the interface location given by equation (5) translates into a Gaussian distribution of the magnetization given by equation (7). So, within this wet regime the width of the Gaussian can easily be measured and the relationship $\chi_L \propto L$ (see equations (7) and (8)) has been verified, as shown in Figure 6. This behavior is similar to that observed in the interface localization-delocalization transition under equilibrium conditions, in both the slit [2,44] and corner geometries [29].

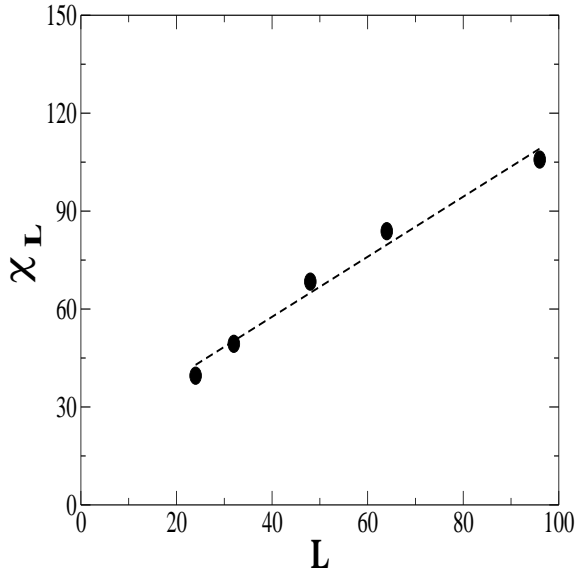


Fig. 6. Plot of χ_L versus L , as obtained from the order parameter probability distribution measured within the wet phase, for $H = 0.8$ and $T = 0.65$.

Decreasing the magnitude of the field, the onset of two distinct maxima shows gradually up (e.g. for $H = 1.8$ in Figure 5), as is also observed in equilibrium systems [2,29,30,44]. Indeed, this behavior not only reflects the fact that the interface is located close to one of both corners with the same probability, but also it is the signature of a thermal continuous phase transition taking place at finite critical temperature [45,46,47]. Finally, well inside the nonwet phase, for $H = 0.5$ in Figure 5), one has an exponential decay of the distribution as already reported for the equilibrium counterpart [29].

Let us now consider the extrapolation of the L -dependent critical points to the $L \rightarrow \infty$ limit, in order to show that the above discussed behavior of the interface is not only characteristic of confined systems, but it is also present in the thermodynamic limit, hence leading to the phase diagram shown in the inset of Figure 3. It is well known that,

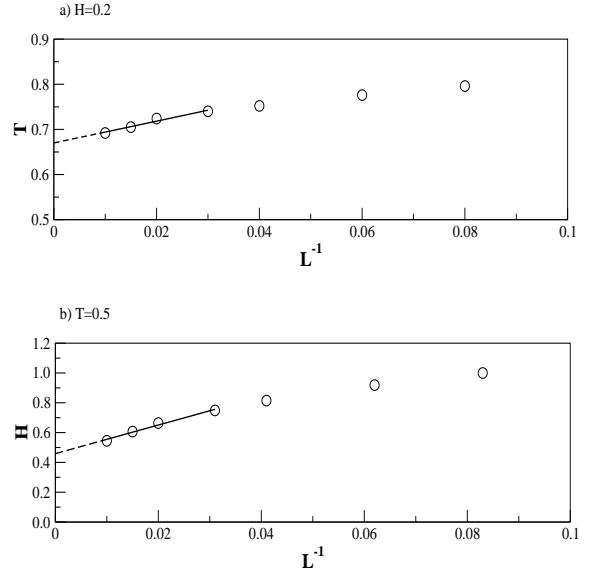


Fig. 7. Extrapolation of the results to the thermodynamic limit: (a) plot of $T_{cw}(L)$ versus L^{-1} , for $H_{cw} = 0.2$, and (b) plot of $H_{cw}(L)$ versus L^{-1} , for $T_{cw} = 0.5$. The extrapolated fits (which take into account the larger lattices only, i.e., $32 \leq L \leq 96$) are also shown.

in the general context of continuous phase transitions, due to finite-size effects the effective location of second-order transitions becomes shifted according to [41]

$$T_c(L) = T_c(\infty) + AL^{-1/\nu}, \quad (12)$$

where $T_c(L)$ is the effective L -dependent “critical” temperature, $T_c(\infty)$ is the actual critical temperature in the thermodynamic limit, A is a constant and ν is the correlation length exponent related to the proper order parameter. In the present case, the location of the interface ($\langle l_o \rangle$), see equation (2), is the appropriated order parameter for the corner wetting transition, rather than the magnetization as in the standard Ising (or MEM) model. The associated correlation length is given by ξ_{\perp} (see equation (3))

describing the growth of correlations in the direction perpendicular to the interface (see Figure 1). For the confined Ising system in the corner geometry under equilibrium one has that the predicted exponent is $\nu_{\perp} = 1$. So, we have performed the extrapolations to the thermodynamic limit by taking $\nu = 1$. Of course, an accurate numerical determination of the exponent is beyond our computational capabilities.

So, let us now apply these concepts to the corner wetting transition of the MEM. Considering the L -dependent critical points $(H_{cw}(L), T_{cw}(L))$ on the localization-delocalization transition curves corresponding to finite systems, we fixed the value of either the magnetic field or the temperature, and extrapolated the results to the $L^{-1} \rightarrow 0$ limit. For the purpose of illustration, Figure 7(a) shows a plot of $T_{cw}(L)$ versus L^{-1} obtained for a fixed value of the magnetic field ($H_{cw} = 0.2$), while Figure 7(b) shows a plot of $H_{cw}(L)$ versus L^{-1} for a fixed value of the temperature ($T_{cw} = 0.5$). Considering only larger lattices (namely, within the range $32 \leq L \leq 96$), the extrapolations allow us to determine the corner wetting transition curve corresponding to the thermodynamic ($L \rightarrow \infty$) limit, which is shown in Figure 3. Deviation from the linear behavior observed for smaller lattices may be due to finite-size corrections or eventually to the fact that the correlation length exponent could slightly depart from unity, as already discussed above. It should be noticed that, as in the case of confined (finite-size) systems, the corner wetting transition (lower curve, solid line) is here compared to the wetting transition of the MEM (upper curve, dashed line)

obtained in Reference [15]. As observed in the confined Ising model [29,44], the critical curve in the case of corner wetting lies also below than that of pure wetting, except for $H = 0$.

After the evaluation of the critical points it is natural to discuss the trends of the magnetization fluctuations upon varying the system size and, subsequently, analyze whether a scaling plot could be obtained. Figure 8(a) shows plots of $\chi(L, T)$ as a function of the temperature obtained for different values of L and keeping constant the surface magnetic field $H = 0.2$. As expected, the different curves exhibit rounding and shifting effects characteristic of finite systems. For the corner wetting transition under equilibrium conditions it is known that the susceptibility of the finite square scales according to [29]

$$\chi(L, T) \propto \frac{L^2}{T} \chi^*(Lt), \quad (13)$$

where χ^* is a scaling function and $t = T - T_{cw}$ (see also equation (10)). So, in the inset of figure 8(a) we show that the maxima of the magnetization fluctuations χ_{max} (measured at $T_{cw}(L)$) of the non-equilibrium counterpart also scales with L^2 . Furthermore, figure 8(b) shows a scaling plot of the magnetization fluctuations according to equation (13). The data shown correspond to $T > T_{cw}$ and the expected asymptotic behavior (dashed-dotted line) is roughly achieved for the larger samples only. Of course, a data collapse of better quality would be desirable but, regrettably, it is beyond our computational capabilities.

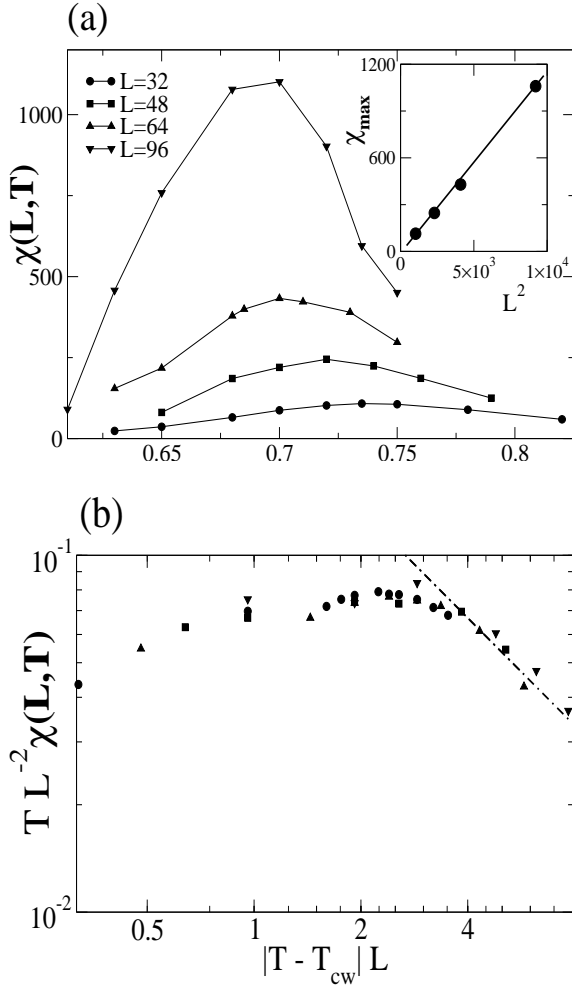


Fig. 8. (a) Plots of the magnetization fluctuations as a function of the temperature obtained for different values of the lattice size, as indicated. The surface magnetic field has been fixed to $H = 0.2$. The inset shows a plot of the maxima of χ versus L^2 . (b) Scaling plot of the data corresponding to the magnetization fluctuations shown in (a) performed according to equation (13). The dashed-dotted line shows the expected asymptotic behavior and has been shown for the sake of comparison.

5 Conclusions

In this work we have studied the phenomenon of corner wetting, observed upon the growth of a magnetic mate-

rial under far-from-equilibrium conditions, using extensive Monte Carlo simulations. The occurrence of this phenomenon was firstly described at a qualitative level, by means of typical snapshot configurations that depend on the control parameters (surface magnetic field and temperature), and subsequently quantitatively, by identifying well defined regions in the $H - T$ phase diagram. After presenting the interface localization-delocalization transition phenomenon in (finite-size) confined geometries, the results were extrapolated to the thermodynamic limit. These results, obtained in the framework of nonequilibrium growth systems, are a novel realization of analogous phenomena, which have recently been observed in equilibrium systems. Hence, we hope that this work will contribute to the understanding of the irreversible growth of binary mixtures in confined geometries, as well as of wetting-related phenomena.

Acknowledgements

This work was financially supported by CONICET, UNLP, and ANPCyT (Argentina).

References

1. P. G. de Gennes, *Rev. Mod. Phys.* **57**, (1985) 827.
2. A. O. Parry and R. Evans, *Phys. Rev. Lett.* **64**, (1990) 439; *Physica A* **181**, (1992) 250.
3. M. R. Swift, A. L. Owczarek, and J. O. Indekeu, *Europhys. Lett.* **14**, (1991) 465.

4. K. Binder, D. P. Landau, and A. M. Ferrenberg, Phys. Rev. Lett. **74**, (1995) 298; Phys. Rev. E **51**, (1995) 2823; Phys. Rev. E **53**, (1995) 5023.
5. A. Maciolek and J. Stecki, Phys. Rev. B **54**, (1996) 1128.
6. A. Maciolek, J. Phys. A (Math. and Gen.) **29**, (1996) 3837.
7. A. Wener, F. Schmid, M. Mueller, and K. Binder, J. Chem. Phys. **107**, (1997) 8175.
8. H. Liu, A. Bhattacharya, and A. Chakrabarti, J. Chem. Phys. **109**, (1998) 8607.
9. A. M. Ferrenberg, D. P. Landau, and K. Binder, Phys. Rev. E **58**, (1998) 3353.
10. H. L. Frisch, S. Puri, and P. Niebala, J. Chem. Phys. **110**, (1999) 10514.
11. M. Müller, E. V. Albano, and K. Binder, Phys. Rev. E **62**, (2000) 5281.
12. D. Sullivan and M. M. Telo da Gama, in *Fluid Interfacial Phenomena*, (Wiley, New York, 1985).
13. S. Dietrich, in *Phase Transitions and Critical Phenomena*, Vol. 12, Eds. C. Domb and J. Lebowitz. (Academic, London, 1988).
14. H. Hinrichsen, R. Livi, D. Mukamel, and A. Politi, Phys. Rev. Lett. **79**, (1997) 2710; Phys. Rev. E **68**, (2003) 041606.
15. J. Candia and E. V. Albano, Phys. Rev. Lett. **88**, (2002) 016103; J. Phys.: Condens. Matter **14**, (2002) 4927.
16. J. Candia and E. V. Albano, J. Chem. Phys. **117** (2002) 6699; J. Magn. Magn. Mater. **260** (2003) 338.
17. E. Cheng and M. W. Cole, Phys. Rev. B **41**, (1990) 9650.
18. M. Napiórkowski, W. Koch, and S. Dietrich, Phys. Rev. A **45**, (1992) 5760.
19. K. Rejmer, S. Dietrich, and M. Napiórkowski, Phys. Rev. E **60**, (1999) 4027.
20. S. Dietrich, in *New Approaches to Old and New Problems in Liquid State Theory - Inhomogeneities and Phase Separation in Simple, Complex and Quantum Fluids*, C. Caccamo, J.P. Hansen, and G. Stell (Eds.), NATO ASI, Ser. B (Kluwer, Dordrecht, 1998), pp.197-244.
21. A. O. Parry, C. Rascón, and A. J. Wood, Phys. Rev. Lett. **83**, (1999) 5535.
22. A. O. Parry, A. J. Wood, and C. Rascón, J. Phys.: Condens. Matter **12**, (2000) 7671.
23. A. O. Parry, A. J. Wood, E. Carlon, and A. Drzewinski, Phys. Rev. Lett. **87**, (2001) 196103.
24. A. O. Parry, M. J. Greenall, and A. J. Wood, J. Phys.: Condens. Matter **14**, (2002) 1169.
25. D. B. Abraham, A. O. Parry, and A. J. Wood, Europhys. Lett. **60**, (2002) 106.
26. D. B. Abraham and A. Maciolek, Phys. Rev. Lett. **89**, (2002) 286101.
27. A. O. Parry, C. Rascón, and A. J. Wood, Phys. Rev. Lett. **85**, (2000) 345.
28. A. O. Parry, A. J. Wood, and C. Rascón, J. Phys.: Condens. Matter **13**, (2001) 4591.
29. E. V. Albano, A. De Virgiliis, M. Müller, and K. Binder, J. Phys.: Condens. Matter **15**, (2003) 333.
30. A. Milchev, M. Müller, K. Binder and D. Landau, Phys. Rev. E **68**, (2003) 031601.
31. G. Timp, in *Nanotechnology*, Springer Verlag, New York, (1999).
32. D. Josel, D. Wheeler, H. W. Huber and T. P. Moffat, Phys. Rev. Lett. **87**, (2001) 16102.
33. A. De Virgiliis, O. Azzaroni, R. C. Salvarezza and E. V. Albano, Appl. Phys. Lett. **82**, (2003) 1953.

34. The subscript π is used to emphasize that this quantity is pertinent to a planar wetting transition.
35. M. E. Fisher, J. Chem. Soc. Faraday Trans. II, **82**, (1986) 1589.
36. M. Ausloos, N. Vandewalle, and R. Cloots, Europhys. Lett. **24**, (1993) 629; N. Vandewalle and M. Ausloos, Phys. Rev. E **50**, (1994) R635.
37. M. Eden, in *Symp. on Information Theory in Biology*, H.P. Yockey (Ed.), Pergamon Press, New York (1958); *Proc. 4th Berkeley Symposium on Mathematics, Statistics and Probability*, F. Neyman (Ed.), University of California Press, Berkeley, Vol.IV, (1961) p.223.
38. J. Candia and E.V. Albano, Eur. Phys. J. B **16**, (2000) 531.
39. J. Candia and E.V. Albano, Phys. Rev. E **63**, (2001) 066127.
40. J. Candia and E. V. Albano, J. Appl. Phys. **90**, (2001) 5395.
41. K. Binder and D. Heermann. *A guide to Monte Carlo simulations in Statistical Physics*. Cambridge, Cambridge University Press. (2000).
42. S. W. Sides, P. A. Rikvold and M. A. Novotny, Phys. Rev. Lett. **81**, (1998) 834.
43. G. Korniss, C. J. White, P. A. Rikvold and M. A. Novotny, Phys. Rev. E **63**, (2001) 016120.
44. E. V. Albano, K. Binder, D. W. Heermann, and W. Paul, Surf. Sci. **223**, (1989) 151.
45. K. Binder, Z. Phys. B: Condens. Matter **43**, (1981) 119.
46. A. D. Bruce, J. Phys. C **14**, (1981) 3667.
47. M. M. Tsy-pin and H. W. J. Blöte, Phys. Rev. E **62**, (2000) 73.

